Electronic Supplementary Information (ESI)

Developing Hierarchically Porous MnO_x/NC Hybrid Nanorods for Oxygen Reduction and Evolution Catalysis

Jay Pandey,[a] Bin Hua,[b] Wesley Ng,[a] Ying Yang,[c] Koen van der Veen,[a] Jian Chen,[d] Norbert J. Geels,[a] Jing-Li Luo,[b] Gadi Rothenberg,[a] and Ning Yan*[a]

[a] *Van `t Hoff Institute for Molecular Sciences, University of Amsterdam, Science Park 904, 1098 XH Amsterdam, The Netherlands E-mail: n.yan@uva.nl, Tel: +31 20 525 6468*

[b] *Department of Chemical and Materials Engineering, University of Alberta, T6G 1K9, Edmonton, AB, Canada*

[c] *Department of Mechanics and Engineering Structure, Wuhan University of Technology, 430070, Wuhan, China*

[d] *National Institute for Nanotechnology, National Research Council of Canada, T6G 2M9, Edmonton, AB, Canada*

This file contains

1. Experimental details
2. Table S1-S2
3. Figure S1-S11

1. Experimental details

1.1 Electrocatalyst synthesis

The electrocatalyst was synthesized using a hydrothermal reaction in a Teflon-lined stainless steel (SS) autoclave. Initially, 2.5 mmol of manganese acetate ($Mn(CH_3COO)_2$, 99% purity, Sigma Aldrich) and 2.5 mmol of nitrotriacetic acid (NTA) ($N(CH_2COOH)_3$, 99% purity, Alfa Aesar) (1:1 mole ratio) were mixed together in 50 ml of de-ionized (DI) water. The suspension was then transferred to the autoclave (total capacity: 75 ml) for a reaction at 180 ^oC for 6 h. The subsequently obtained white thick slurry was centrifuged (2600 rpm for 15 min) and washed several times with ethanol and DI water to get the white powder followed by drying at 80 ^oC for 6 h. Three sets of reaction were done to give sufficient MnNTA yield. In the pyrolysis step, approximately 1.5g of MnNTA powder was placed in a quartz tube, pyrolyzed at 900 ^oC under argon (99.99% purity) atmosphere for 1 h. The heating rate was 10 $^oC\ min^{-1}$ and the Ar flow rate was 130 ml min^{-1}. The yield of MnO/NC was approximately 400 mg. In the final step of mild calcination, MnO/NC powder was well dispersed in an alumina crucible, and oxidized in static air at 200 ^oC in a furnace. The final MnO_x/NC hybrid rods contained ~20 wt% NC and ~80 wt% MnO_x.

The synthesis of MnO_x rod was prepared by calcinating MnNTA rods in air at 900 for 1 h which produced Mn_2O_3 nanorods. The obtained rods were reduced in 5 % H_2 +N_2 at 800 ^oC for 15 min to yield MnO rods. After a similar 200 ^oC-oxidation, MnO_x rods were acquired. The MnO_x/C composite was acquired by mixing MnO_x rods and carbon black during the ink preparation, as detailed below.

The synthesis of NC also used NTA-based precursor according to our previous work.[1,2] Briefly, potassium and magnesium cations were employed to adjust the nitrogen content in NC. The formed NC precursor contained 32 mol.% of HMgNTA and 68mol.% of KMgNTA. The final NC was doped with ~ 1.4 at.% of N, which was comparable with the N content in MnO_x/NC (1.5 at.%).

1.2 Electrochemical procedures

We have prepared five catalyst inks in the experiments, consisting of commercial Pt/C (20 wt % Pt on Vulcan XC 72, fuel cell grade, Premetek, USA), commercial Ru/C (5 wt% Ru, reduced, Alfa Aesar), NC, MnO_x/NC and MnO_x/C. In a typical preparation excluding MnO_x/C: 1 ml ethanol, 10 µL Nafion® (D-521 dispersion 5 wt % in water/isopropanol, Alfa Aesar 42117) and 1 mg powder were mixed in a vial and sonicated overnight. For the preparation of MnO_x/C ink, 1.5 mg power and 0.5 mg of

carbon black were added to the ink before sonication. The subsequently obtained MnO_x/C contained 20 wt% carbon, identical with that of the MnO_x/NC hybrid.

Dropcasting was applied to prepare the rotating disc electrode (RDE, glassy carbon electrode, Gamry, USA) with a diameter equaled to 5 mm (A = 0.196 cm2). Initially, the RDE was polished sequentially by diamond polishing films with 1 and 0.1 μm particles (Allied High Tech Products, USA) with water rinse. Inks were then dropcasted by 5 μL portions x 6, with air drying in between. The total catalyst loading was 30 μg, or 153 μg/cm^2 for all catalyst except for MnO_x/C which was 306 μg/cm^2).

Electrochemical experiments were performed in a classic 3-electrode setup. 0.1 M KOH solution, stabilized at 25.0 ± 0.1 °C in a water bath, was used as the electrolyte. A Gamry Reference 600 potentiostat was employed, together with a Gamry RDE710 rotating electrode setup. Saturated calomel electrode (SCE, Gamry, USA) separated from the solution by a 10 cm bridge was used as a reference electrode, and a graphite rod (Gamry, USA) as a counter electrode. Potentials were reported vs. reversible hydrogen electrode (RHE) in all cases by adding 1.011 for pH 13. Nitrogen (99.999%) or oxygen (99.999%) were bubbled for 30 minutes to saturate the solution, and were flowed above the solution ('gas blanket') during the experiments. In ORR measurements, the linear scan voltammograms (LSV) were obtained with a scan rate of 10 mV s^{-1} at rotating speeds of 400, 600, 900, 1200, 1600, 2000 and 2400 rpm. In OER, the rotating speed was fixed at 1600 rpm. Cyclic voltammetry was measured with the same parameters but without rotation.

The solution resistance was determined initially, and 90% of the value (typically 30–50 Ohm) was used as a positive correction factor in an automatic iR drop correction in voltammetric and chronoamperometric measurements. CV was performed between 0.8 to 1.2 V vs. RHE to measure the capacitive current for all the examined catalysts, and a post-measurement correction was applied. The ORR chronoamperometry was performed at the approximately the half-wave potential of the catalyst. In the methanol resistance study, 20 mL methanol was injected into the electrolyte to yield a roughly 3 M methanol concentration.

1.3 Koutecký-Levich plots

The number of electrons transferred in the reaction was estimated by the Koutecký-Levich equation:[3]

$$\frac{1}{J} = \frac{1}{B\omega^{-1/2}} + \frac{1}{J_K}$$

Where J is the measured current density (mA cm^{-2}), J_K is the kinetic (exchange) current density (mA cm^{-2}), ω is the RDE rotation rate (rpm), and B is given by:

$$B = 0.2nFC_O D_O^{2/3} \nu^{-1/6}$$

Where 0.2 is the arithmetic correction factor for ω in rpm, n is the number of electrons transferred per mol, F is Faraday's constant, C_O is the concentration of dissolved O_2 (1.2 mmol ml^{-1} at 25 °C in 0.1 M KOH), D_O is the diffusion coefficient of O_2 ($1.9 \cdot 10^{-5}$ cm^2 s^{-1} at 25 °C in 0.1 M KOH), and υ is the kinematic viscosity of the 0.1 M KOH electrolyte at 25 °C (0.01 cm^2/s). By plotting $1/J$ versus $\omega^{-1/2}$ at different potentials and fitting linear equations to the data, the number of electrons (n) could be calculated from the slope ($1/B$).

1.4 Materials characterizations

X-Ray diffraction (XRD) patterns were obtained using a MiniFlex II diffractometer equipped with CuKα radiation. The X-ray tube was operated at 30 kV and a current of 5 mA. Nitrogen adsorption isotherms where measured on a Thermo Scientific Surfer instrument at 77 K. The sample was dried in vacuum (1×10^{-3} mbar) for 3 h at 200 °C prior to the measurement. Temperature programmed reduction (H_2-TPR) was performed on a Thermo TPDRO-1100 instrument equipped with a thermal conductivity detector (TCD). 10~15 mg of the catalyst was loaded to the quartz tube reactor, and all the measurements were carried out in a stream of 5% H_2 in N_2 (40 ml min^{-1}) with a heating rate of 10 K min^{-1}. Thermogravimetric analysis (TGA) coupled with differential scanning calorimetry (DSC) was performed using a NETZSCH Jupiter® STA 449F3. All the measurements were done in the temperature range 30-900 °C under the air atmosphere with flow rate of 20 ml min^{-1} at a heating rate of 5 K min^{-1}.

Scanning electron microscope (FEI Verios 60 with ETD detector) was used to observe the morphology of the samples. Transmission electron microscope (TEM) analysis was performed using a JEOL 2200 FS TEM. X-ray photoelectron spectroscopy (XPS) was carried out using a Kratos AXIS equipped with a monochromatic Al Kα X-ray source. The base pressure in the analytical chamber was maintained at 10^{-9} mbar. The obtained spectra were analyzed using the Thermo Avantage software calibrated to the C 1s binding energy of 285.0 eV. For curve fitting and deconvolution, a Shirley-type background subtraction and a Gaussian-Lorentzian peak shape were applied. In the assignment of nitrogen functionalities, we avoided using the pyrrolic, because they are known to decompose at temperatures above 800 °C to either pyridinic or graphitic nitrogen.[4, 5]

Table S1. Performance comparison of selected excellent non-noble metal ORR catalyst reported recently. All the data were recorded in alkaline condition with a rotation speed of 1600 rpm. Note that all the mateials, other than MnO_x/NC, were only reported ORR active.

Journal name, Year	Catalyst	$E_{orr-1/2}$ (V vs. RHE)	Ref.
Angewandte Chem. Int. Ed., 2016	Co-N_x single-atom site	0.88	6
J. Am. Chem. Soc., 2015	graphene quantum dots	~0.82	7
This work	**MnO_x/NC**	**0.80**	
Nano Energy, 2016	Co_3O_4-Mn_3O_4/GO composite	0.78	8
Adv. Funct. Mater., 2016	$PrBa_{0.85}Ca_{0.15}MnFeO_{5+\delta}$	0.77	9
Angewante Chem. Int. Ed., 2015	nitrogen-doped carbon	0.74	10
Adv. Mater., 2016	Co/N contained CNT	0.73	11
Nat. Commun., 2015	$Co_{3-x}Mn_xO_4$	0.73	12
Chem. Commun., 2015	N-doped carbon dots	0.71	13
Angewante Chem. Int. Ed., 2016	λ-$MnO_{2-\delta}$	0.67	14
ChemSusChem, 2016	MnO_2/m-ZSM-5	0.56	15

Table S2. Performance and synthesis comparisons of selected excellent non-noble metal oxygen bifunctional catalyst reported recently. Other than specified, all the data were recorded in alkaline condition with a rotation speed of 1600 rpm.

Journal name, Year	Catalyst	Key Precursors and Methods	$E_{orr-1/2}$ (V vs. RHE)	E_{oer-10} (V vs. RHE)	ΔE (V)	Ref.
Angewandte Chem. Int. Ed., 2016	$Co@Co_3O_4$/N doped CNT	metal-oganic framework (ZIF-67)	0.80	1.65	0.85	16
This work	**MnO_x/NC**	**hydrothermal synthesis**	**0.80**	**1.67**	**0.87**	
Energ. Environ. Sci., 2016	Co_9S_8/N-graphene	hydrothermal + NH_3 plasma teatments	0.75	1.64	0.89	17
J. Am. Chem. Soc., 2016	Nano structured α-MnO_2	$KMnO_4$ and hydrothermal synthesis	0.79	1.72	0.93	18
Energ. Environ. Sci., 2016	$Co_{25}Zn_{75}$-C1100	ZIF-8 metal-organic framework	0.81	1.74	0.93	19
J. Am. Chem. Soc., 2014	amorphous $CoFe_2O_{\sim 3.66}$	hydrothermal synthesis	0.76	1.72	0.96	20
Angewante Chem. Int. Ed., 2014	Mn_xO_y/NC	porphyrins and phthalocyanines	~0.71[a]	1.68	0.97	21
Chem. Commun., 2015	$Ni_{0.6}Co_{2.4}O_4$ film on Ni foil	electrodeposition	0.77	1.76	0.99[b]	22
Appl. Catal. B-Environ., 2017	$NiCoMnO_4$/N-rGO	graphene oxide + NH_4NO_3 treatment	0.75	~1.75[c]	1.00	23
J. Am. Chem. Soc., 2010	Mn oxides	electrodeposition	0.73	1.77	1.04	24
Catal. Sci. Technol., 2016	Mn_2O_3 nanoballs	Hydrothermal sysnthesis	0.67[c]	1.81[c]	1.24	25

[a] the value was extimated from the LSV curve.

[b] LSV was perofrmed at 2500 rpm.

[c] these values were extimated from the corresponding LSV curves.

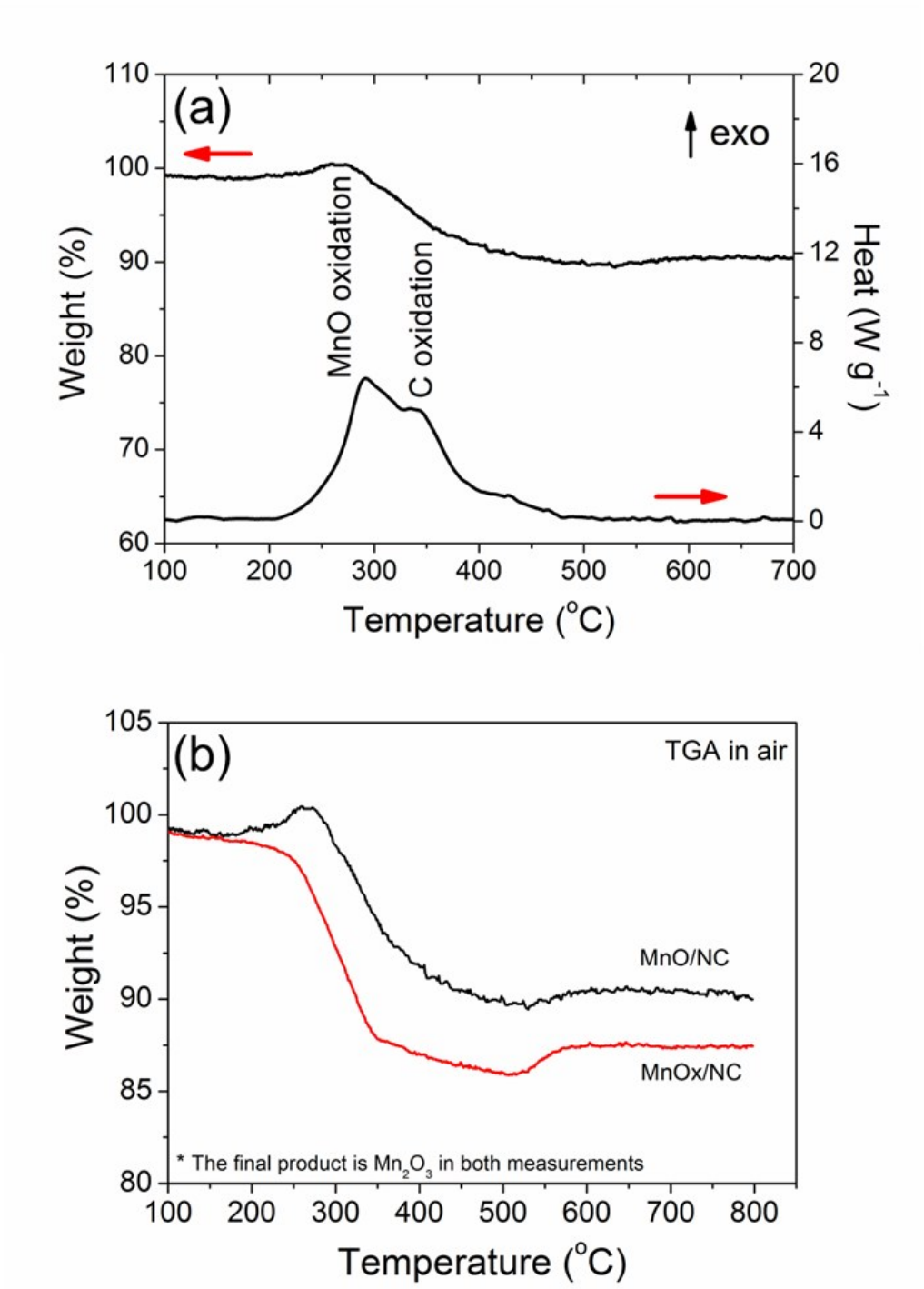

Figure S1. (a) TGA-DSC curve of MnO/NC in air; (b) a comparison of TGA curves for MnO_x/NC and MnO/NC in air.

The first weight increase associated with a exothermic peak was ascribed to the oxidation of MnO in MnO_x. Carbon was not oxidized during the 200 °C oxidation treatment.

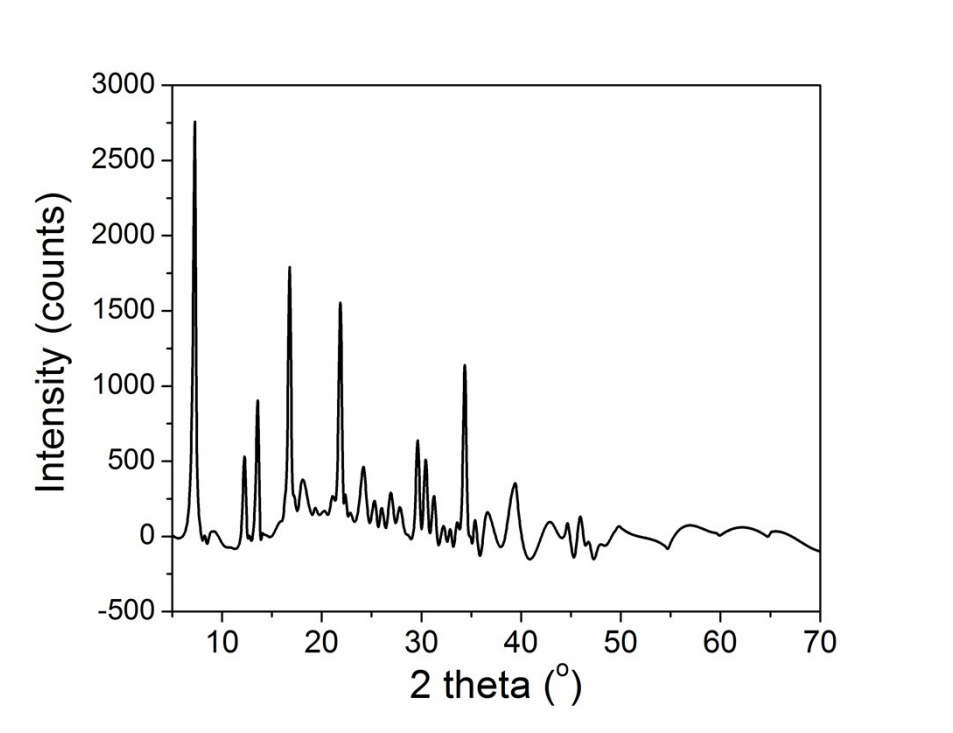

Figure S2. XRD pattern of MnNTA salt before pyrolysis.

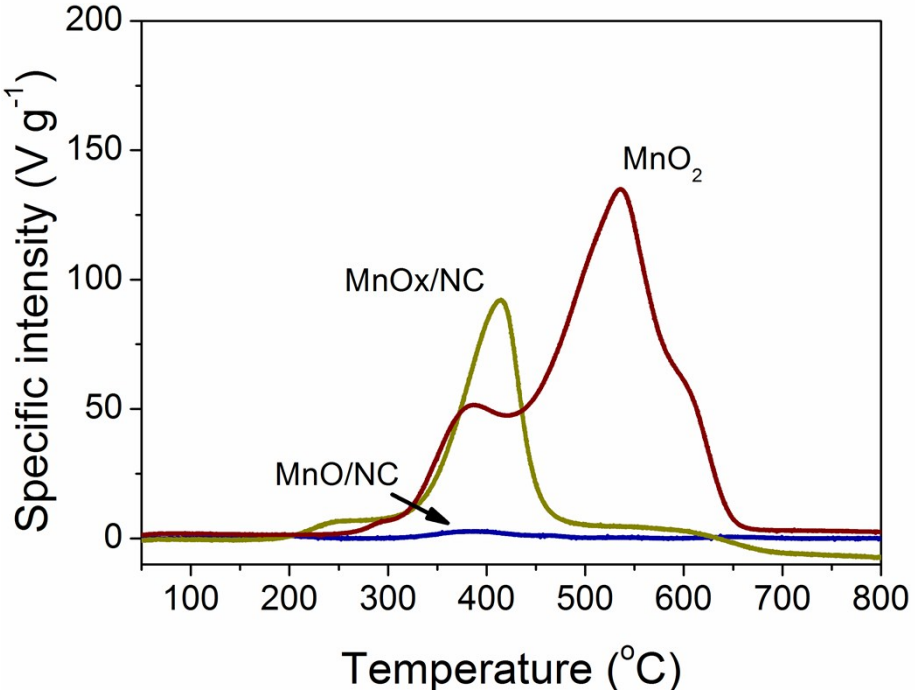

Figure S3. H_2-TPR spectra of MnO/NC and MnO_x/NC, commercial MnO_2 was used as a reference. The signal was normalized to the specific intensity (V g^{-1}). Here, note that all the manganese oxides were reduced to MnO in 5% H_2 + N_2 at 800 °C.

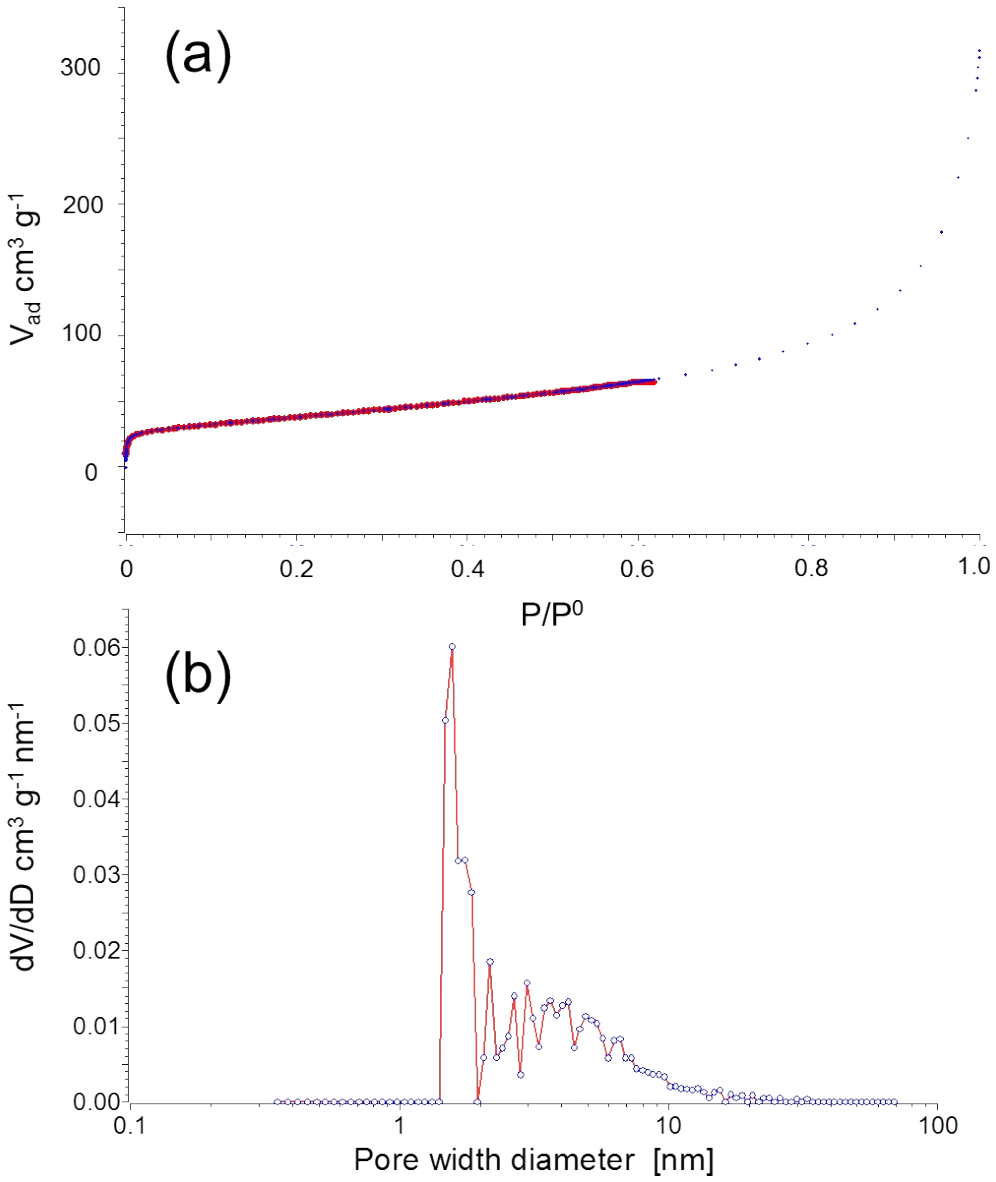

Figure S4. (a) The nitrogen adsorption isotherm of MnO_x/NC (blue dotted line) and and the simulated isotherm calculated using NLDFT method (red solid line); (b) The pore size distribution calculated using NLDFT method.

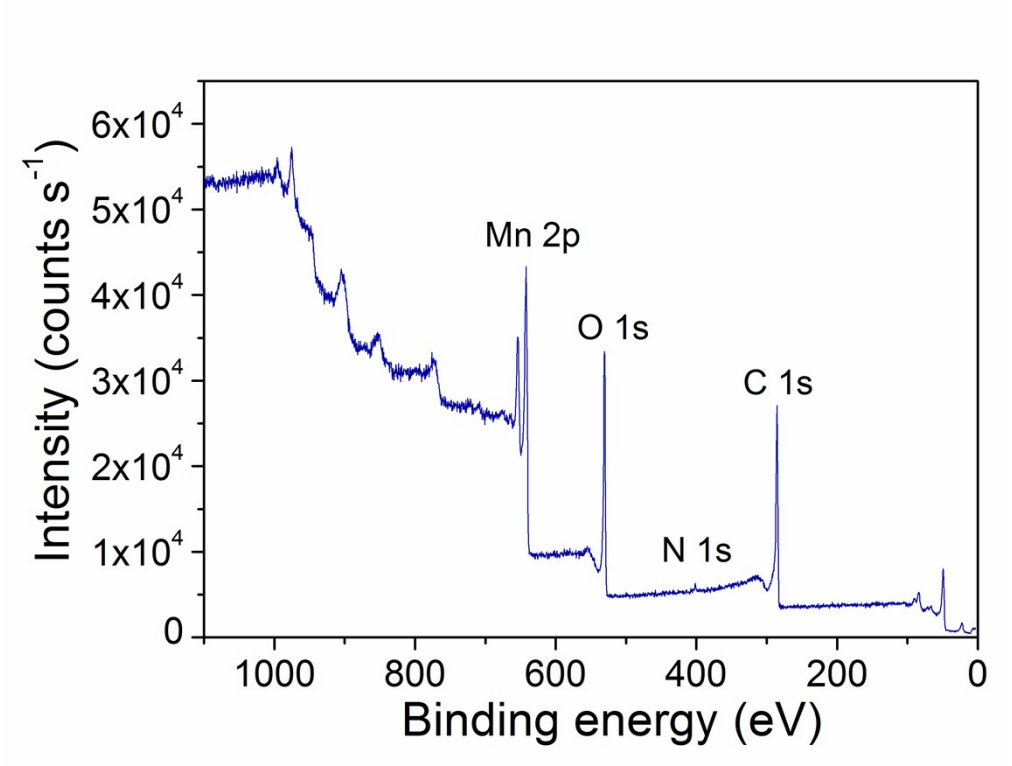

Figure S5. XPS survey spectrum of MnO_x/NC.

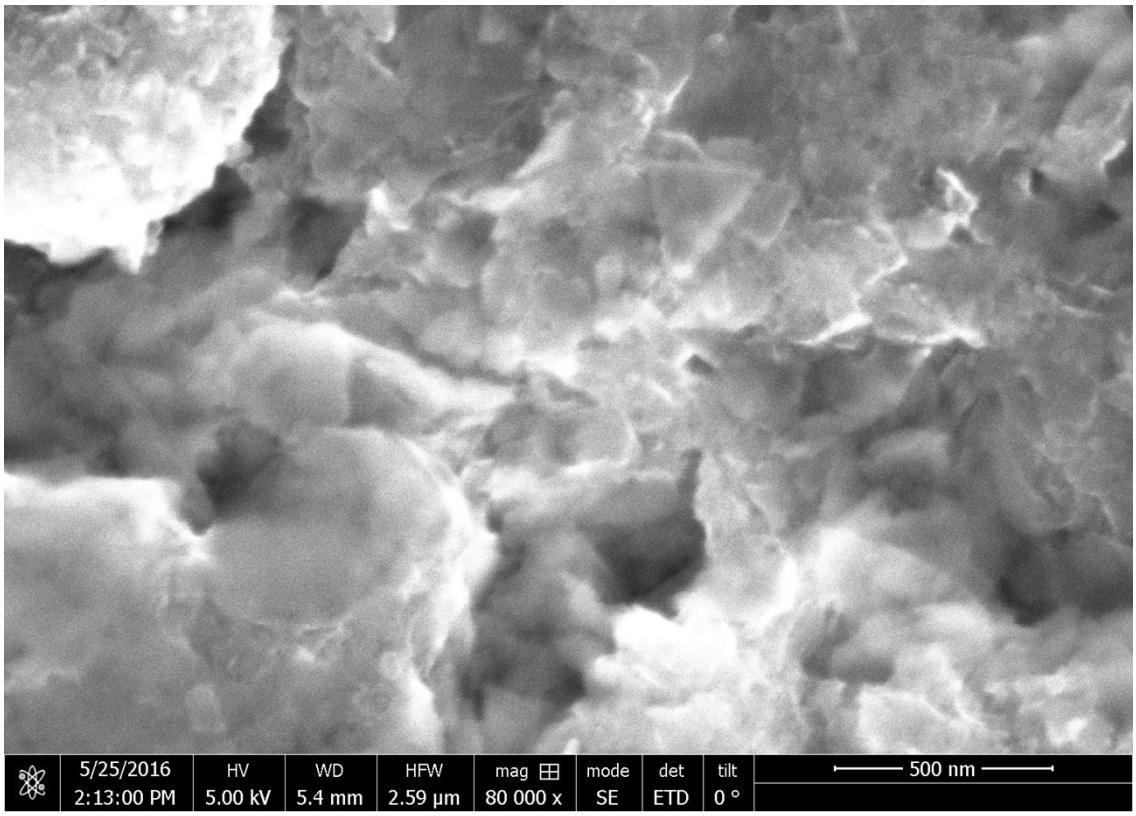

Figure S6. SEM image of the carbon hybrid derived using iron (instead of Mn) NTA salt.

No rod-like structure was seen. Similarly, we have not observed the nanorod structure in Mg based NTA salt (see our previous work in refs. 1 and 2)

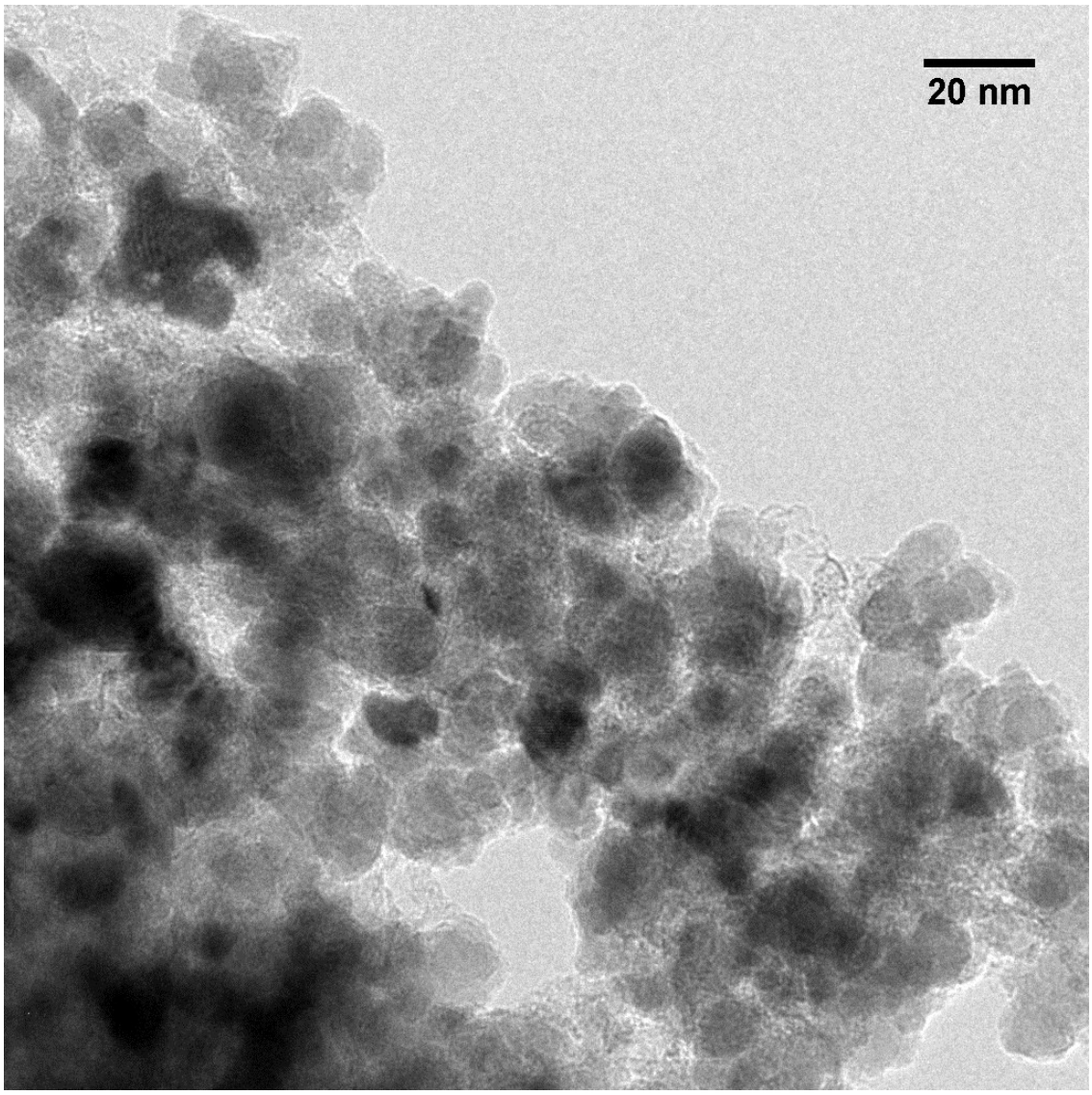

Figure S7. TEM image of the surface of MnO_x/NC. All manganese oxide nanoparticles were well connected by the 3D carbon network.

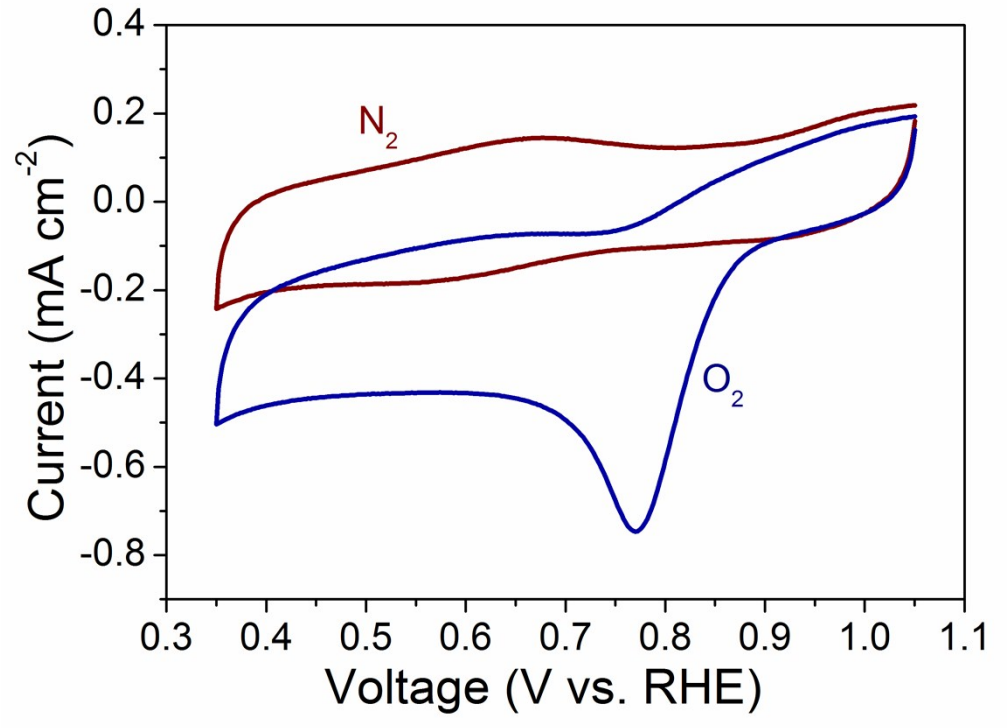

Figure S8. CV plots of MnOx/NC in both oxygen and nitrogen saturated electrolyte. The scan rate was 10 mV s^{-1}.

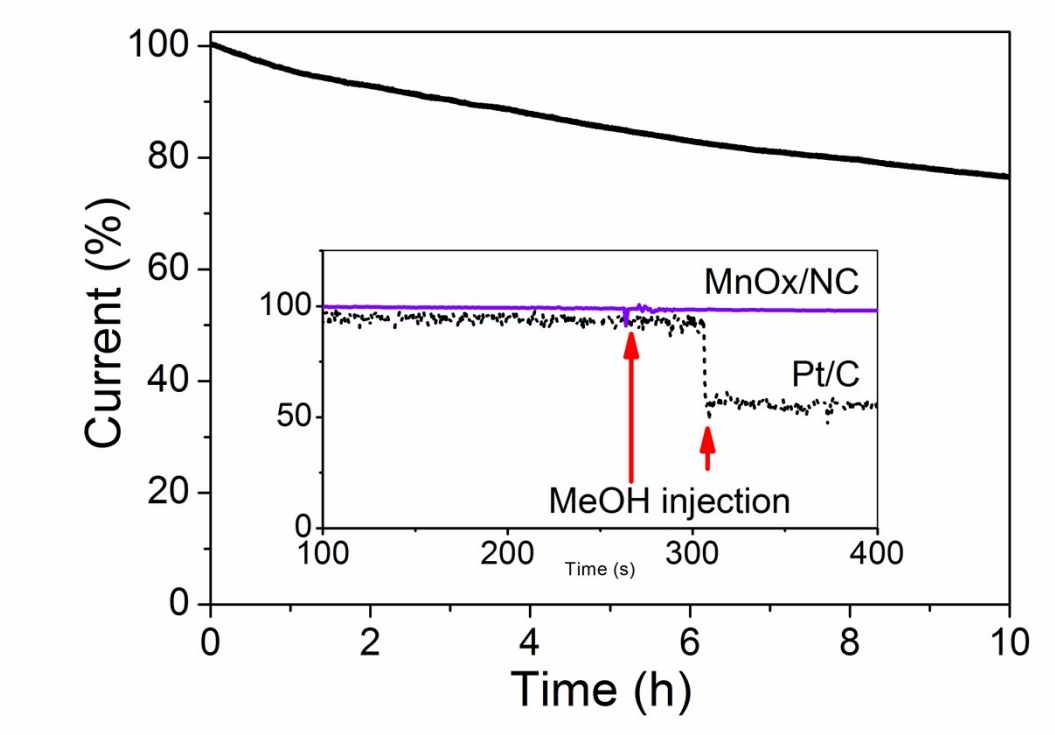

Figure S9. Chronoamperometric stability testing of MnO_x/NC at a constant voltage of 0.8 V vs. RHE and 600 rpm, while bubbling O_2; the inset compared current variation of MnO_x/NC and commercial Pt/C when 20 ml methanol was injected (the final methanol concentration was ~ 3M).

Note that the catalyst shows merely *ca.* 20 % current loss in the methanol-poisoned electrolyte after 10 h test.

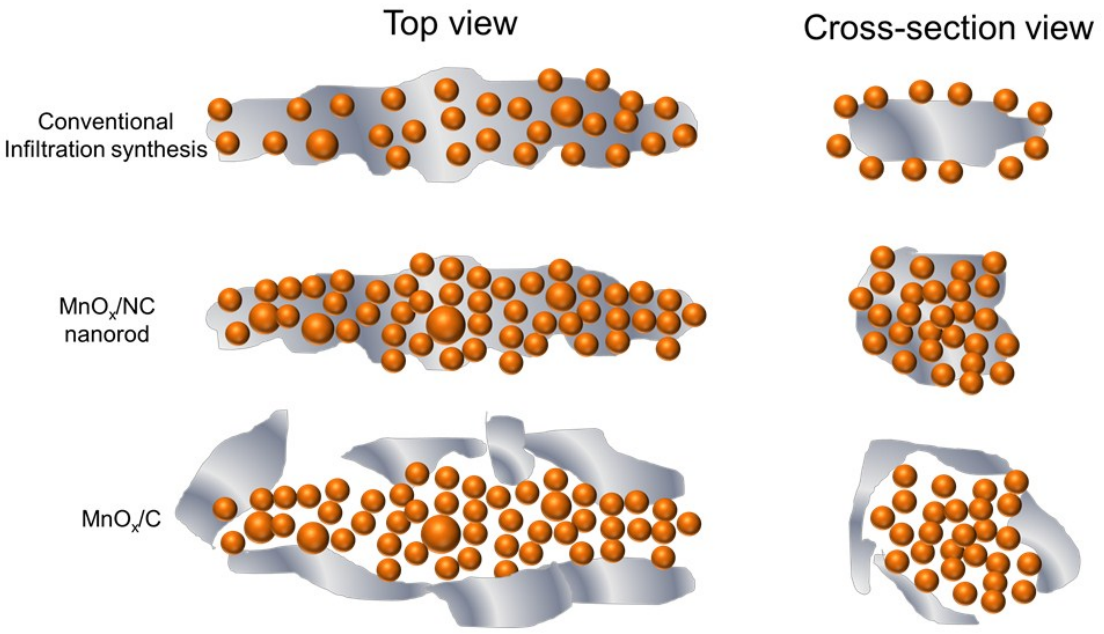

Figure S10. A schematic structural comparison of carbon supported MnO_x catalyst preparation by the infiltration method, MnO_x/NC nanorod hybrid and MnO_x/C (the control).

The conventional carbon supported MnO_x catalyst preparation by infiltration method indeed demonstrated excellent electrical conductivity. However, the Mn loading is relatively low and the inner park of the carbon sheet is inactive (see the cross-sectional view), both restricting its electrocatalytic potency.

Thanks to the 3D percolated NC network, MnO_x/NC hybrid owned 80% MnO_x nanoparticles which were all electrochemically active. Together with the active NC, it demonstrated excellent bifunctional activity.

In the control group (MnO_x/C), the high loading did not create more "valid" active sites. This is simply because of the poor electrical conductivity of MnO_x, which caused the low activity of the inner-part MnO_x.

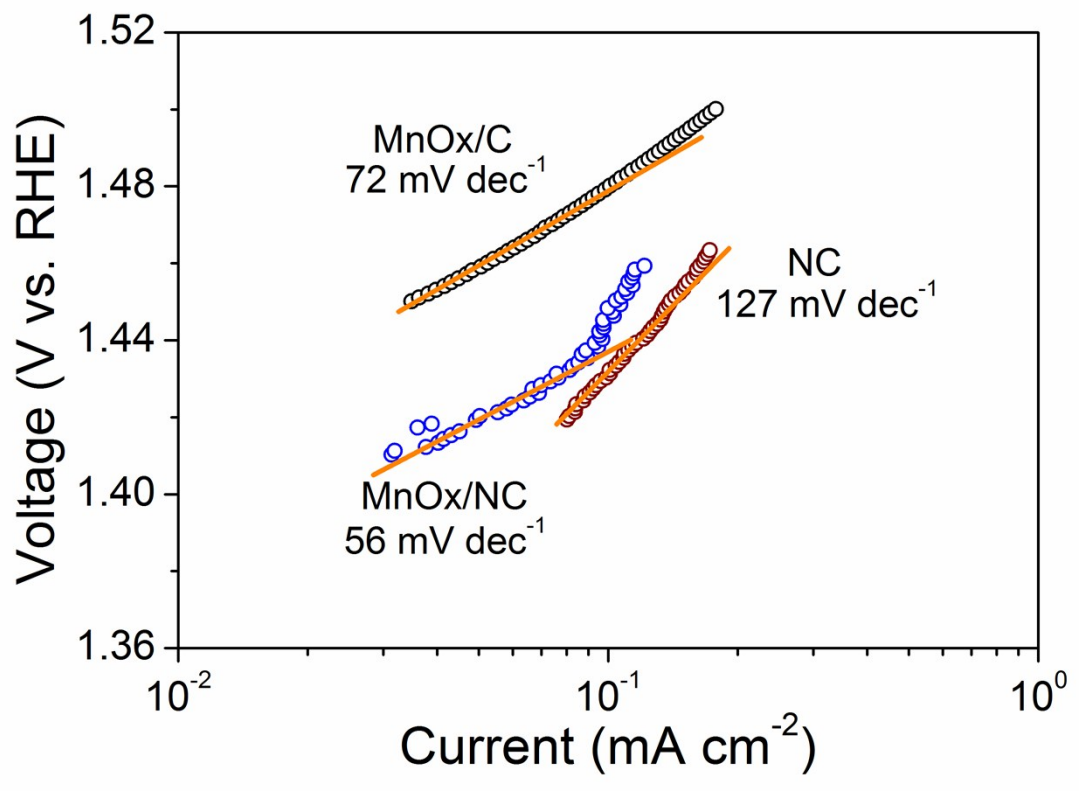

Figure S11. OER Tafel plots of NC, MnO_x/C and MnO_x/NC catalysts. All the plots were derived from the corresponding LSV plots at 1600 rpm.

References

[1] D. Eisenberg, W. Stroek, N. J. Geels, C. S. Sandu, A. Heller, N. Yan, G. Rothenberg, *Chem. Eur. J.*, **2016**, 22, 501-505.

[2] D. Eisenberg, W. Stroek, N.J. Geels, S. Tanase, M. Ferbinteanu, S.J. Teat, P. Mettraux, N. Yan and G. Rothenberg, *Phys. Chem. Chem. Phys.*, **2016**, 18, 20778-20783.

[3] A. J. Bard, L. R. Faulkner, *Electrochemical Methods: Fundamentals and Applications*, John Wiley & Sons, **2001**.

[4] J. R. Pels, F. Kapteijn, J. A. Moulijn, Q. Zhu, K. M. Thomas, *Carbon* **1995**, *33*,

[5] G. Wu, P. Zelenay, *Acc. Chem. Res.* **2013**, *46*, 1878–1889.

[6] P. Q. Yin, T. Yao, Y. Wu, L. R. Zheng, Y. Lin, W. Liu, H. X. Ju, J. F. Zhu, X. Hong, Z. X. Deng, G. Zhou, S. Q. Wei and Y. D. Li, *Angew. Chem. Int. Ed.*, **2016**, 55, 10800-10805.

[7] H. Jin, H. Huang, Y. He, X. Feng, S. Wang, L. Dai, J. Wang, *J. Am. Chem. Soc.,* **2015**, *137*, 7588–7591.

[8] L. J. Dai, M. Liu, Y. Song, J. J. Liu and F. Wang, *Nano Energy*, **2016**, 27, 185-195.

[9] B. Hua, Y. Q. Zhang, N. Yan, M. Li, Y. F. Sun, J. Chen, J. Li and J. L. Luo, *Adv. Funct. Mat.*, **2016**, 26, 4106-4112.

[10] J. Tang, J. Liu, C. Li, Y. Li, M. O. Tade, S. Dai, Y. Yamauchi, *Angew. Chem. Int. Ed.,* **2015**, 588–593.

[11] Z. Y. Lu, W. W. Xu, J. Ma, Y. J. Li, X. M. Sun and L. Jiang, *Adv. Mat.*, **2016**, 28, 7155-7161.

[12] C. Li, X. Han, F. Cheng, Y. Hu, C. Chen and J. Chen, *Nat. Commun.*, **2015**, 6, 7345.

[13] C. Hu, C. Yu, M. Li, X. Wang, Q. Dong, G. Wang, J. Qiu, *Chem. Commun.,* **2015**, *51*, 3419–3422.

[14] S. Lee, G. Nam, J. Sun, J. S. Lee, H. W. Lee, W. Chen, J. Cho and Y. Cui, *Angew. Chem. Int. Ed.*, **2016**, 55, 8599-8604.

[15] X. Cui, Z. Hua, L. Chen, X. Zhang, H. Chen and J. Shi, *ChemSusChem*, **2016**, 9, 1010-1019.

[16] A. Aijaz, J. Masa, C. Rosler, W. Xia, P. Weide, A. J. R. Botz, R. A. Fischer, W. Schuhmann and M. Muhler, *Angew. Chem. Int. Ed.*, **2016**, 55, 4087-4091.

[17] S. Dou, L. Tao, J. Huo, S. Y. Wang and L. M. Dai, *Energ. Environ. Sci.*, **2016**, 9, 1320-1326.

[18] Y. T. Meng, W. Q. Song, H. Huang, Z. Ren, S. Y. Chen and S. L. Suib, *J. Am. Chem. Soc.*, **2014**, 136, 11452-11464.

[19] S. Gadipelli, T. Zhao, S. A. Shevlin and Z. Guo, *Energ. Environ. Sci.*, **2016**, 9, 1661-1667.

[20] A. Indra, P. W. Menezes, N. R. Sahraie, A. Bergmann, C. Das, M. Tallarida, D. Schmeisser, P. Strasser and M. Driess, *J. Am. Chem. Soc.*, **2014**, 136, 17530-17536.

[21] J. Masa, W. Xia, I. Sinev, A. Q. Zhao, Z. Y. Sun, S. Grutzke, P. Weide, M. Muhler and W. Schuhmann, *Angew. Chem. Int. Ed.*, **2014**, 53, 8508-8512.

[22] T. N. Lambert, J. A. Vigil, S. E. White, D. J. Davis, S. J. Limmer, P. D. Burton, E. N. Coker, T. E. Beechem and M. T. Brumbach, *Chem. Commun.,* **2015**, 51, 9511-9514.
[23] A. Pendashteh, J. Palma, M. Anderson and R. Marcilla, *Appl. Catal. B*, **2017**, 201, 241-252.
[24] Y. Gorlin and T. F. Jaramillo, *J. Am. Chem. Soc.*, **2010**, 132, 13612-13614.
[25] S. Ghosh, P. Kar, N. Bhandary, S. Basu, S. Sardar, T. Maiyalagan, D. Majumdar, S. K. Bhattacharya, A. Bhaumik, P. Lemmens and S. K. Pal, *Catal. Sci. Tech.*, **2016**, 6, 1417-1429.